Self-Assembly of Cubes into 2D Hexagonal and Honeycomb Lattices by Hexapolar Capillary Interactions

SUPPLEMENTARY MATERIAL

Giuseppe Soligno,[1] Marjolein Dijkstra,[2] and René van Roij[1]

[1] *Institute for Theoretical Physics, Center for Extreme Matter and Emergent Phenomena, Utrecht University, Princetonplein 5, Utrecht 3584 CC, The Netherlands*

[2] *Soft Condensed Matter, Debye Institute for Nanomaterials Science, Department of Physics and Astronomy, Utrecht University, Princetonplein 5, Utrecht 3584 CC, The Netherlands*

I. SINGLE-ADSORBED CUBE

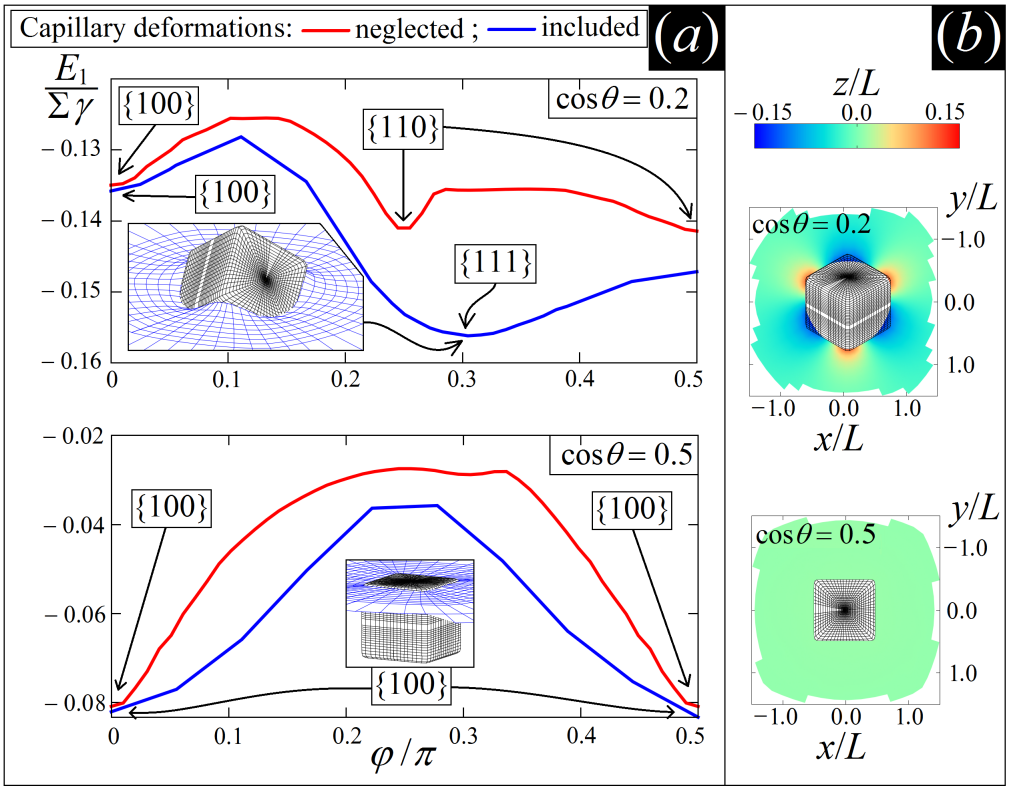

Figure S1: (a): E_1 (Eq. (1)) of a cubic particle, with side L and Young's contact angle θ, at a fluid-fluid interface, minimized over the particle's center of mass height z_c and the particle's internal Euler angle ψ, as a function of the particle's polar angle φ (see Fig. 1(a)), for $\cos\theta = 0.2$ and $\cos\theta = 0.5$, in units of $\Sigma\gamma$, with Σ the cube's total surface area and γ the fluid-fluid surface tension. The blue lines are the results obtained through our numerical method [43], which includes capillary deformation effects. The red lines are the results obtained through the TTT [45], i.e. neglecting capillarity. The labels {100}, {110} and {111} indicate the cube's orientations in each minimum of the energy (see Fig. 1(c)). In the insets we show, for the particle equilibrium configurations, a 3D view of the interface shape (blue grid) close to the particle (black grid), as calculated by our method. (b): Contour plots for the minimum-energy configuration of the cube of the deformed-interface height profile, as obtained by our numerical method, for the two Young's angles considered. The plane $z = 0$ corresponds to the fluid-fluid interface when no particle is adsorbed.

II. TWO-ADSORBED CUBES

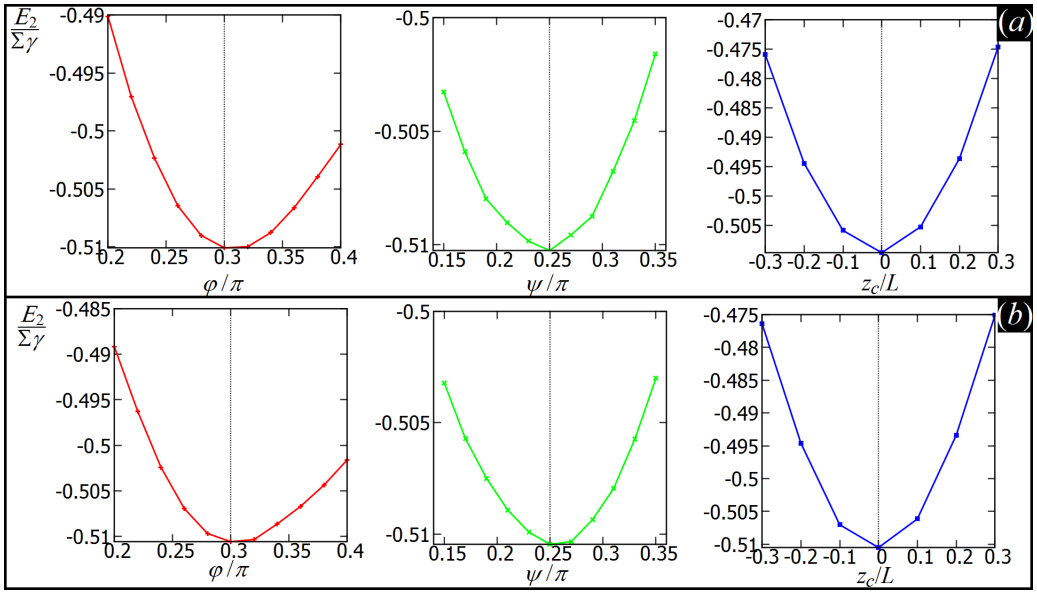

Figure S2: Adsorption energy E_2 (Eq. (1)) for a system of two adsorbed cubes (with side L, surface area Σ, contact angle $\theta = 90°$) at a distance $D = 1.6\,L$ (i.e. close to the contact distance) and with reciprocal azimuthal orientations such that they are (a) dipole-dipole and (b) tripole-tripole interacting. The equilibrium configuration of each cube is the minimum-energy $\{111\}$ configuration shown in Fig. 1 for $\theta = 90°$. Here we plot the energy E_2 (in units of $\Sigma\gamma$, with γ the fluid-fluid surface tension) obtained by varying the value of, respectively, φ, ψ and z_c (see Fig. 1) for one of the two cubes. The vertical dotted line represent the equilibrium value in the $\{111\}$ configuration. This proves that capillary interactions between two cubes do not affect the equilibrium configuration $\{111\}$ of each cube that we calculated for a single-adsorbed cube.

III. MANY-ADSORBED CUBES

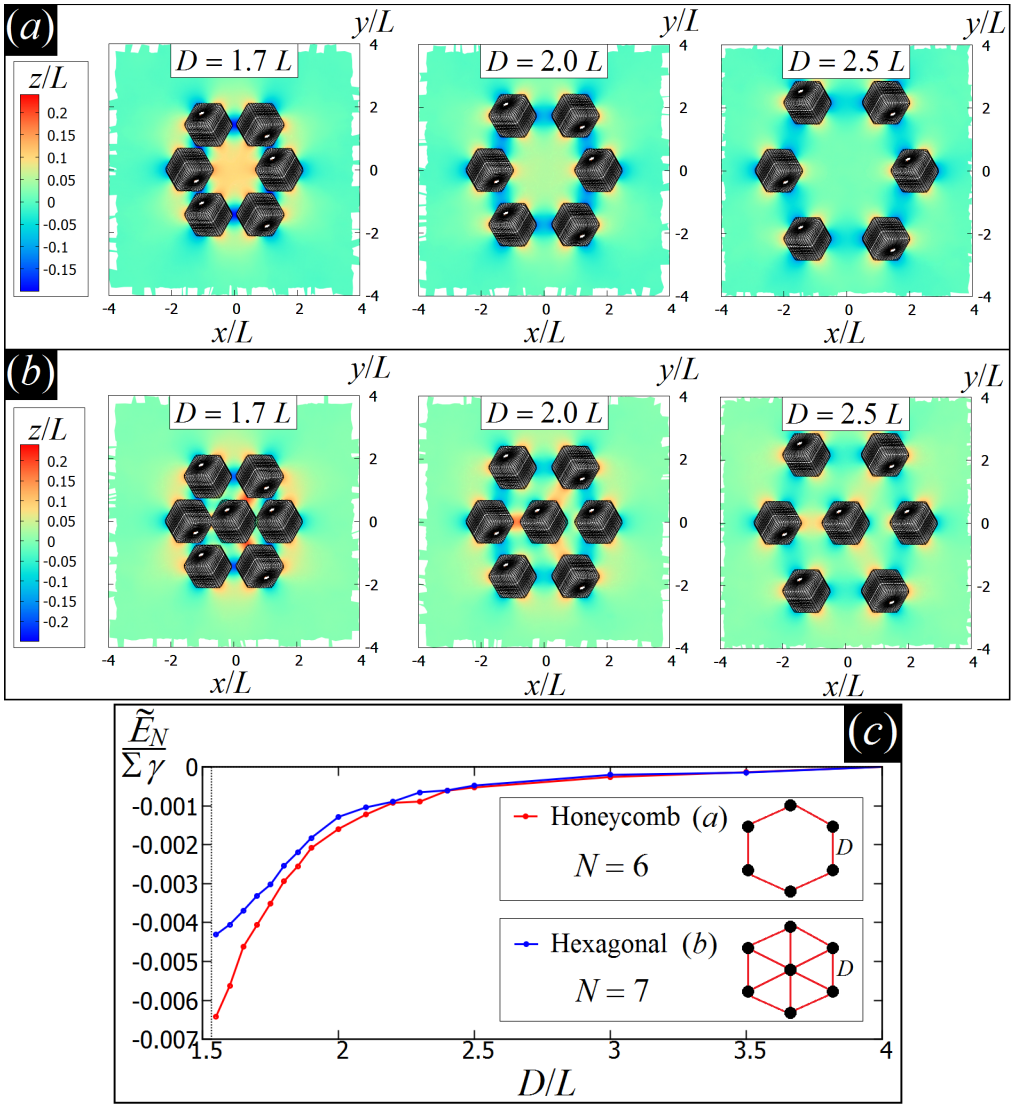

Figure S3: Results for adsorbed {111}-oriented cubes with side L, surface area $\Sigma \approx 6L^2$, and Young's contact angle $\theta = 90°$. The fluid-fluid surface tension is γ. (a)-(b): Contour plots of the interface height profile, as obtained through our numerical method, for $N = 6$ and $N = 7$ adsorbed cubes, respectively, for various center-of-mass particle distances D. The azimuthal orientations of the cubes are such that the cubes interact through the tripole-tripole attachment (see also Fig. 2). The plane $z = 0$ corresponds to the interface when no particle is adsorbed. (c): Interaction energy per particle $\tilde{E}_N$ (Eq. (2)) for $N = 6$ and $N = 7$ adsorbed and tripole-tripole interacting cubes. As shown, $\tilde{E}_N$ for the 6-particle system (i.e. corresponding to the honeycomb assembly, see (a)) is lower than for the 7-particle system (i.e. corresponding to the hexagonal assembly, see (b)). Therefore tripole-tripole interacting cubes prefer to assemble into a honeycomb lattice and not into a hexagonal one. As a matter of fact, in the hexagonal assembly (see (b)) the central cube cannot attach through an attractive tripole-tripole interaction with all its six neighbors, but it is forced to experience repulsive interaction with some of them.

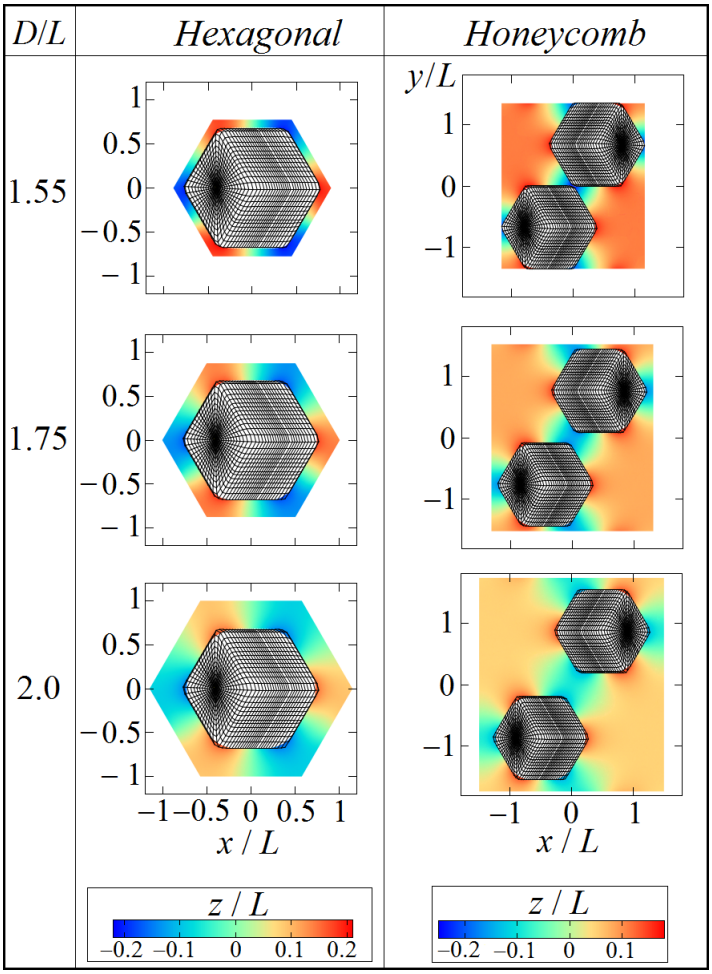

Figure S4: Contour plots of the interface height profile, as obtained through our numerical method, for the unit cells of the hexagonal and honeycomb lattices (see also Fig. 2) corresponding to different center-of-mass particle distances D. Each cube has side L, contact angle $\theta = 90^\circ$, total surface area $\Sigma \approx 6L^2$, and it is adsorbed at its equilibrium configuration (i.e. the {111} configuration, see Fig. 1). The plane $z = 0$ corresponds to the interface when no particle is adsorbed.

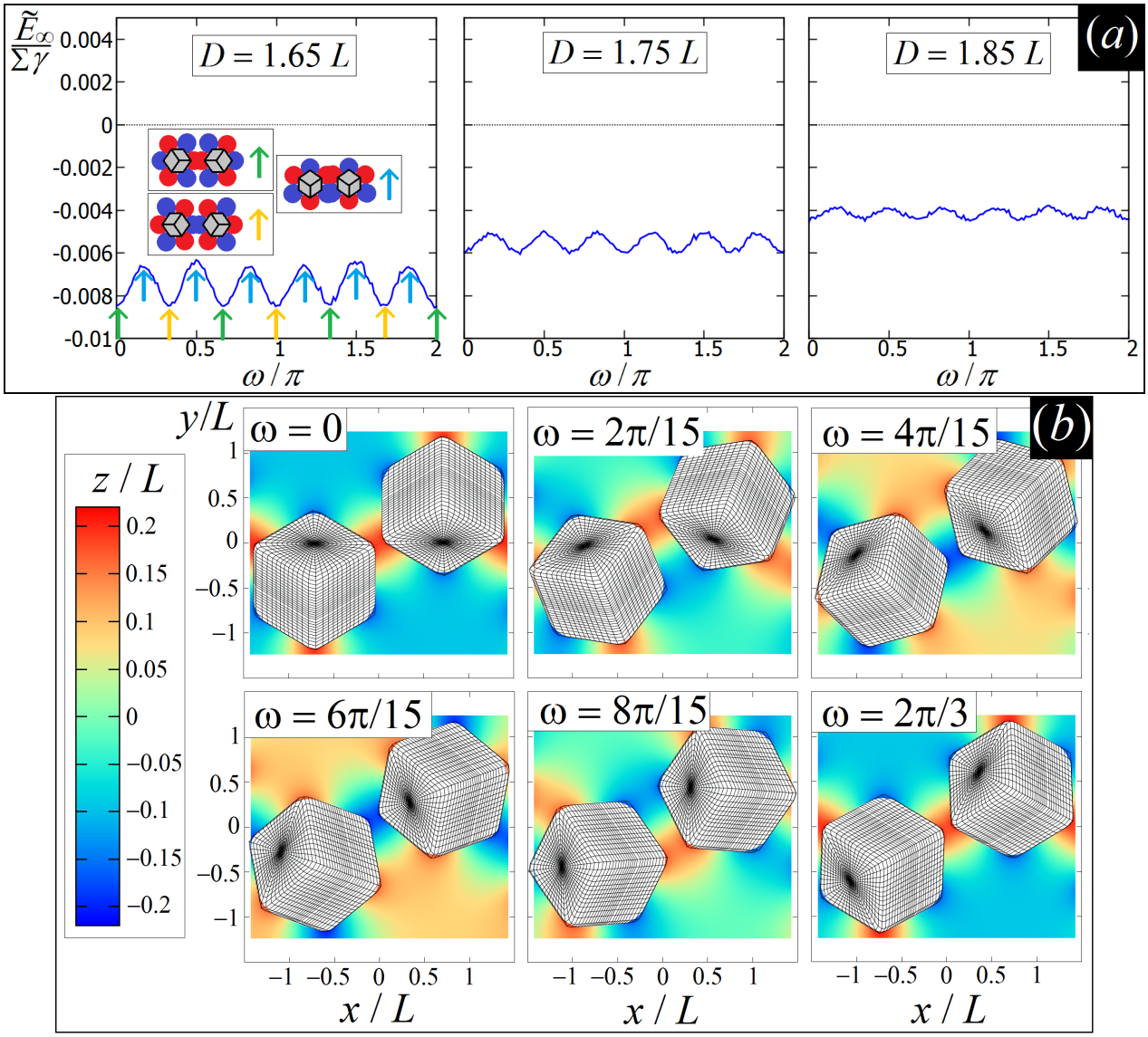

Figure S5: (a) Interaction energy per particle $\tilde{E}_\infty$ (Eq. (2)) for an honeycomb lattice of adsorbed {111}-oriented cubes (with side L, contact angle $\theta = 90^\circ$, total surface area $\Sigma \approx 6L^2$, at a center-of-mass distance D from each other, and for a fluid-fluid surface tension γ) with respect to the rotation ω of the azimuthal orientation of the cube from equilibrium. Each cube is rotated in the opposite angular direction with respect to its neighbors. In this way, by tuning ω, the cubes shift from tripole-tripole to dipole-dipole attachments. As indicated by the colored arrows in the left graph (and the analogous behavior holds in the other two graphs), for the honeycomb lattice the tripole-tripole attachment is energetically more favorable than the dipole-dipole attachment. This suggests that, to evolve from a honeycomb lattice with tripole-tripole interacting cubes to an hexagonal lattice with dipole-dipole interacting cubes, an energy barrier exists, because the hexagonal lattice is stable only for dipole-dipole attachments (see Fig. S3), and therefore the honeycomb should first replace the tripole-tripole bonds with dipole-dipole bonds. (a) Contour plot of the interface height profile, as obtained through our numerical method, for the unit cell of the honeycomb lattice, for $D = 1.65\,L$ and different values of ω (see (a)). The plane $z = 0$ corresponds to the interface when no particle is adsorbed.

IV. TEMPERATURE-DENSITY PHASE DIAGRAM CALCULATIONS

In Fig. 2(d) we show the capillary interaction energy per particle $\tilde{E}_\infty$ (Eq. (2)), for adsorbed {111}-oriented cubes assembled into a honeycomb lattice with tripole-tripole attachments and into a hexagonal lattice with dipole-dipole attachments, with respect to the lattice spacing. The hexagonal lattice reaches the minimum $\tilde{E}_\infty$, and therefore it is a candidate for the equilibrium structure. However the honeycomb lattice has a lower density than the hexagonal lattice. Therefore, for certain temperatures and densities, the cubes could prefer the former phase, if the configurational entropy is taken into account. To verify this, we define for the cubes a free energy where both entropic and capillary contributions are included. Firstly, we assume that the adsorbed cubes can have three possible phases: a disordered fluid phase, a honeycomb-lattice crystal phase with the cubes tripole-tripole interacting, and a hexagonal-lattice crystal phase with the cubes dipole-dipole interacting. We indicate the free energy of these three phases as F_f, F_h and F_x, respectively.
In the fluid phase, we assume that our {111}-oriented adsorbed cubes behave like an hard-disk fluid. That is

$$F_f \approx F_{hd}^{(f)} \,, \tag{S1}$$

where $F_{hd}^{(f)}(N, A, T)$ is the free energy of a fluid phase of N hard disks of radius R in a 2D space of total area A and at a temperature T. Using the standard "Taylor expansion" scaled-particle theory [53], we can write

$$\frac{F_{hd}^{(f)}}{A\,(k_B T)} = \frac{N}{A}\left[\ln\left(\frac{N}{A}\pi R^2\right) - 1\right] - \frac{N}{A}\ln\left(1 - \frac{N}{A}\pi R^2\right) + \frac{(2\pi R\, N/A)^2}{4\pi(1 - \pi R^2\, N/A)} \,, \tag{S2}$$

where the first term is the entropic ideal-gas contribution and the rest is due to the hard-disk interactions. In our approximated model, the area and perimeter of the hard disk become the area and perimeter of the cube-flat interface intersection, obtaining

$$(2\pi R)^2 \approx 3.07\Sigma \,, \tag{S3}$$

and

$$\pi R^2 \approx 0.23\Sigma \,, \tag{S4}$$

with Σ the cube total surface area. Note that Eq. (S3) implies $R \approx 0.279\sqrt{\Sigma}$, while Eq. (S4) implies $R \approx 0.271\sqrt{\Sigma}$. This slight inconsistence occurs because we are treating our adsorbed cubes as hard disks. We introduce the normalized density $\vartheta^* \equiv \vartheta/\vartheta_x$, where $\vartheta \equiv \Sigma N/A$ and $\vartheta_x \approx 3.24$ is the closest packing value of ϑ for an hexagonal-lattice phase, i.e. when the dipole-dipole interacting cubes are at their contact distance. So, for a system of N adsorbed cubes, we obtain

$$\frac{F_f}{A\,\gamma} = \frac{k_B T}{\Sigma\,\gamma}\vartheta_x\left[\vartheta^* \ln\left(\frac{0.23\vartheta^*}{1/\vartheta_x - 0.23\vartheta^*}\right) - \vartheta^* + \frac{3.07(\vartheta^*)^2}{4\pi(1/\vartheta_x - 0.23\vartheta^*)}\right] \,. \tag{S5}$$

In Eq. (S5) we are not including the capillary-interaction contribution to the energy. Therefore the fluid phase holds for cubes at a rather low density (such that particle-particle distances are, on average, big enough to make the capillary interactions negligible) or for cubes with a random azimuthal orientation of their vertical axis (such that they exert both attractive and repulsive capillary interactions to each other, giving on average a negligible contribution to the total energy). Hard disk systems freeze for a system area lower than $1.328\,A_0$ [54], with $A_0 \equiv 2N\sqrt{3}R^2$ the closest packing area for hard disks with radius R. In our approximate analogy for the {111}-oriented adsorbed cubes, this corresponds to $\vartheta^* > 1/1.328$, so we estimate that Eq. (S5) is reliable for $\vartheta^* < 0.75$.
For the cubes in the honeycomb-lattice phase we assume that

$$F_h \approx N\,\tilde{E}_N^{(h)} - N\,k_B T \ln Z_{or}^{(h)} + F_{hd}^{(f)} \tag{S6}$$

where $\tilde{E}_N^{(h)}$ is the capillary-interaction energy per adsorbed cube (Eq. (2)) for the honeycomb lattice with tripole-tripole interacting cubes, and it is computed through our numerical method. The second term is the entropic contribution per cube to the free energy due to the cube azimuthal orientations. Indeed, in this lattice phase, any i-th cube has a fixed azimuthal orientation α_i of its vertical axis. We assume that the cubes can experience only small angular variations ω in α_i, with an energy cost $U(\omega) \approx C_h(\vartheta^*)\,\omega^2/2$, where the rotational spring constant $C_h(\vartheta^*)$ depends on

the honeycomb lattice density ϑ^*. Using this approximation, the orientation partition function $Z_{or}^{(h)}$ of a single cube can be written as

$$Z_{or}^{(h)} = \frac{3}{2\pi}\int_{-\pi/3}^{\pi/3} e^{-U(\omega)/k_BT}\, d\omega = \frac{3}{4}\sqrt{\frac{2\,k_BT}{\pi\, C_h(\vartheta^*)}}\,\xi\left[C_h(\vartheta^*)\right]\,, \tag{S7}$$

where

$$\xi\left[C_h(\vartheta^*)\right] \equiv 2\,\mathrm{Erf}\left[\frac{\pi}{3}\sqrt{\frac{1}{2}\frac{C_h(\vartheta^*)}{\Sigma\gamma}\frac{\Sigma\,\gamma}{k_BT}}\right]\,, \tag{S8}$$

and $\mathrm{Erf}(x)$ is the "error function". As shown in Fig. S8, for the whole range of parameters that we consider, $\xi\left[C_h(\vartheta^*)\right] \approx 2$, such that the integral in Eq. (S7) is actually a Gaussian one. In Eq. (S7), the factor 3 and the integration between $[-\pi/3, \pi/3]$ takes into account that, for any i-th cube, there are three equivalent minimum-energy azimuthal orientations, which are α_i, $\alpha_i + 2\pi/3$, and $\alpha_i + 4\pi/3$. So from Eq. (S6), expressing $F_{hd}^{(f)}$ by Eq. (S2) analogously to the fluid phase case, we obtain for the honeycomb-lattice free energy

$$\frac{F_h}{A\,\gamma} = \vartheta_x\vartheta^*\frac{\tilde{E}_N^{(h)}}{\Sigma\,\gamma} + \vartheta_x\frac{k_BT}{\Sigma\,\gamma}\left[\vartheta^*\ln\left(\frac{0.23\vartheta^*}{1/\vartheta_x - 0.23\vartheta^*}\right) - \vartheta^* + \frac{3.07(\vartheta^*)^2}{4\pi(1/\vartheta_x - 0.23\vartheta^*)} + \frac{\vartheta^*}{2}\ln\left(\frac{2\pi}{9}\frac{C_h(\vartheta^*)}{\Sigma\gamma}\frac{\Sigma\,\gamma}{k_BT}\right)\right]\,. \tag{S9}$$

The closest-packing value of ϑ^* for the honeycomb lattice, i.e. when the tripole-tripole interacting cubes are at their contact distance, is about $1.83/\vartheta_x$.

Finally, for the hexagonal-lattice solid phase we assume that

$$F_x \approx N\,\tilde{E}_N^{(x)} - N\,k_BT\ln Z_{or}^{(x)} + F_{hd}^{(x)}\,, \tag{S10}$$

where $\tilde{E}_N^{(x)}$ is the capillary-interaction energy per adsorbed cube (Eq. (2)) for the hexagonal lattice with dipole-dipole interacting cubes, and it is computed through our numerical method, the second term is the azimuthal orientation entropic contribution per cube to the free energy and it is calculated analogously to the honeycomb-lattice case, $F_{hd}^{(x)}(N, A, T)$ is the entropic free energy of a solid phase of N hard disks with radius R in a 2D space of total area A and at a temperature T. Following ref. [54], we can write

$$F_{hd}^{(x)} = Nk_BT\left[2.73\ln\left(\frac{A_0}{A}\right) - 2\ln\left(1 - \frac{A_0}{A}\right) + 2.33\frac{A}{A_0} - 0.75\left(\frac{A}{A_0}\right)^2 - 1.475\right]\,, \tag{S11}$$

where $A_0 = 2\sqrt{3}NR^2$ is the closest-packing area for N disks. For our cubes in the hexagonal-lattice phase we use $A_0/A = \vartheta^*$, so for F_x we obtain

$$\frac{F_x}{A\,\gamma} = \vartheta_x\vartheta^*\frac{\tilde{E}_N^{(x)}}{\Sigma\,\gamma} + \vartheta_x\frac{k_BT}{\Sigma\,\gamma}\left[2.73\,\vartheta^*\ln\vartheta^* - 2\,\vartheta^*\ln\left(1-\vartheta^*\right) + 2.33 - \frac{0.75}{\vartheta^*} - 1.475\vartheta^* + \frac{\vartheta^*}{2}\ln\left(\frac{2\pi}{9}\frac{C_x(\vartheta^*)}{\Sigma\gamma}\frac{\Sigma\,\gamma}{k_BT}\right)\right]\,, \tag{S12}$$

where $C_x(\vartheta^*)$ is the rotational spring constant for the hexagonal lattice.

In Fig. S9 we show the behavior of $F_f(\vartheta^*)/A\gamma$ (Eq. (S5)), $F_h(\vartheta^*)/A\gamma$ (Eq. (S9)), and $F_x(\vartheta^*)/A\gamma$ (Eq. (S12)) for several values of $\Sigma\gamma/k_BT$, where Σ is the cube surface area and γ the fluid-fluid surface tension.

For the hexagonal-lattice and honeycomb-lattice phases, we calculated $\tilde{E}_N^{(x/h)}(D)$ (Eq. (2)) in the limit $N \to \infty$ by applying our numerical method to, respectively, an hexagonal lattice unit cell with side $D/\sqrt{3}$ and $N = 1$ cube, and a rectangular lattice unit cell $\sqrt{3}D \times 3D/2$, with $N = 2$ cubes, and with periodic boundary conditions shifted of half-side along the longest side (see Fig. 2(b)-(d)). With D we refer to the center-of-mass distance between two closest-neighbor cubes. The value of ϑ^* for the hexagonal and honeycomb lattices is related to D by $\vartheta^* = 2\Sigma/(\vartheta_x D^2\sqrt{3})$ and $\vartheta^* = 4\Sigma/(3\vartheta_x\sqrt{3}D^2)$, respectively.

To calculate the rotational spring constant C_h for the honeycomb lattice with tripole-tripole interacting cubes, we calculated

$$E_\infty^{*\,(h)} \equiv 2\left(\tilde{E}_\infty^{(h)}(\omega) - \tilde{E}_\infty^{(h)}\right) \tag{S13}$$

for a honeycomb lattice unit cell where the two cubes have azimuthal orientation of their vertical axis given by α_1 and $\alpha_2 + \omega$, respectively. With α_1 and α_2 we refer to the minimum-energy azimuthal orientations that the two tripole-tripole interacting cubes have in the unit cell of the honeycomb-lattice phase, and $\tilde{E}_\infty^{(h)}$ is the capillary-interaction energy per cube (Eq. (2)) when the two cubes have such orientations. With $\tilde{E}_\infty^{(h)}(\omega)$ we refer to $\tilde{E}_\infty^{(h)}$ calculated when the second cube has orientation $\alpha_2 + \omega$. In Fig. S6(a) we show $E_\infty^{*\,(h)}(\omega)$ for several fixed D, as obtained by our numerical method. In Fig. S6(b) we show the values of $C_h(\vartheta^*)$ obtained by fitting $E_\infty^{*\,(h)}(\omega)$ for each ϑ^* considered, in a neighborhood of $\pm\pi/10$ around each minimum in ω, with the function $U_h(\omega) = a_h(\vartheta^*) + \omega^2\, C_h(\vartheta^*)/2$. Then, as shown, we can fit these values using $C_h(\vartheta^*) = A\, e^{-B\,\vartheta^*}$, with $A = 0.021\,\Sigma\gamma$ and $B = 2.70$.
To calculate the rotational spring constant C_x for the hexagonal lattice with dipole-dipole interacting cubes, we proceeded analogously to the honeycomb case, but calculating

$$E_7^{*(x)} \equiv 7\left(\tilde{E}_7^{(x)}(\omega) - \tilde{E}_7^{(x)}\right)\,, \tag{S14}$$

for $N = 7$ cubes, where 6 of them are placed with their center of mass at the vertexes of a side-D hexagon, and the 7th cube is placed at the center of this hexagon. So the minimum-energy azimuthal orientation of these cubes is such that they dipole-dipole interact with each other. In Fig. S7(a) we show $E_7^{*(x)}(\omega)$ for several fixed D, as obtained by our numerical method, where ω is the rotation of the azimuthal orientation of the central cube from its equilibrium value. The terms $\tilde{E}_7^{(x)}$ and $\tilde{E}_7^{(x)}(\omega)$ are the capillary-interaction energy per cube (Eq. (2)) when $\omega = 0$ and $\omega \neq 0$, respectively. In Fig. S7(b) we show the values of $C_x(\vartheta^*)$ obtained by fitting $E_7^{*(x)}(\omega)$, in a neighborhood of $\pm\pi/10$ around each minimum in ω, with the function $U_x(\omega) = a_x(\vartheta^*) + \omega^2\, C_x(\vartheta^*)/2$. Then, as shown, we can fit these values using $C_x(\vartheta^*) = A\, e^{-B/\vartheta^*}$, with $A = 55.30\,\Sigma\gamma$ and $B = 6.71$.
In Fig. S9 we plot, for some values of $\Sigma\gamma/k_BT$, $F_f(\vartheta^*)/A\gamma$ (Eq. (S5)), $F_h(\vartheta^*)/A\gamma$ (Eq. (S9)), and $F_x(\vartheta^*)/A\gamma$ (Eq. (S12)), showing the common tangents between these curves, when present.
In Fig. 3 we report the phase diagram for the adsorbed cubes with respect to $\Sigma\gamma/k_BT$ and ϑ^*, obtained by calculating the common tangents present between $F_f(\vartheta^*)/A\gamma$, $F_h(\vartheta^*)/A\gamma$, and $F_x(\vartheta^*)/A\gamma$ for many different values of $\Sigma\gamma/k_BT$. The temperature range goes from $\Sigma\gamma = 1300\,k_BT$ to $\Sigma\gamma = 300\,k_BT$, as this was the meaningful part of the diagram. As expected, the results predict for $T \to 0$ that the system phase separates for any ϑ^*, collapsing into a hexagonal-lattice phase and leaving the rest of the interface empty. For $\Sigma\gamma/k_BT$ within, about, 350 and 650, we predict the presence of the honeycomb-lattice phase, which can be uniform in the whole system, or coexist with the hexagonal-lattice phase or with the disordered-fluid phase, depending on the global density of the system.

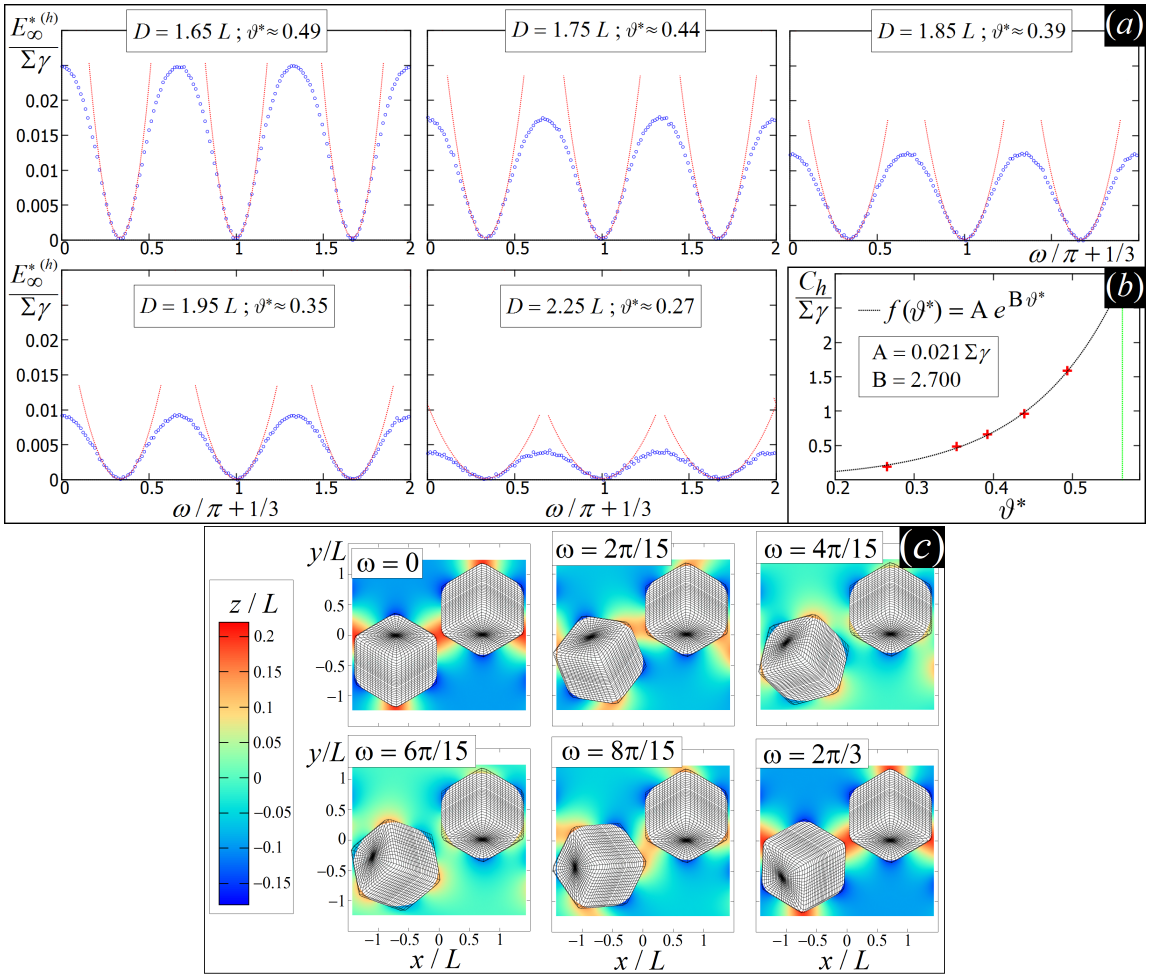

Figure S6: (a) Energy $E_\infty^{*\,(h)}$ (Eq. (S13)) for an honeycomb-lattice unit cell with tripole-tripole interacting cubes, where the azimuthal orientation of the vertical axis of one cube is rotated by ω from its equilibrium value, for several values of the center-of-mass distance D between the two cubes. The cube contact angle is 90°, the cube total surface Σ, and the cube side L. The red dotted curves represent the fit around each minimum of $E_\infty^{*\,(h)}$ with $a_h(\vartheta^*) + \omega^2\, C_h(\vartheta^*)/2$. ($b$) Values of $C_h(\vartheta^*)$, as obtained for the various D considered. The dotted curve is the fit of these values using $A\, e^{B\,\vartheta^*}$. The green vertical line corresponds to $1.83/\vartheta_x$, i.e. the value of ϑ^* for the honeycomb-lattice phase at its closest-packing density. (c) Contour plots of the interface height profile, as obtained through our numerical method, for the honeycomb-lattice unit cell in the case $D = 1.65\, L$ and for different values of ω. The plane $z = 0$ correspond to the fluid-fluid interface when no cubes are adsorbed.

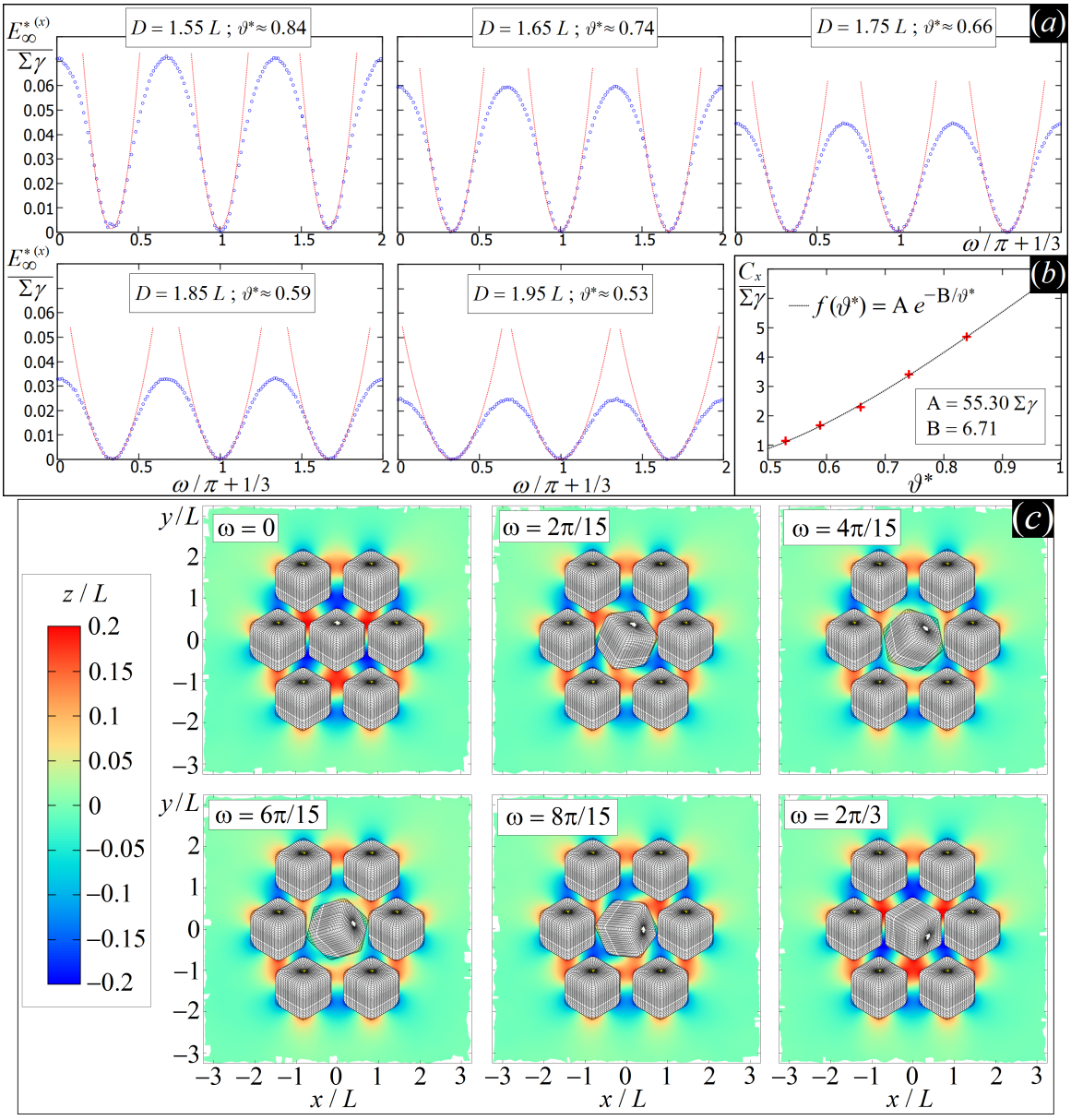

Figure S7: (a) Energy $E_7^{*(x)}$ (Eq. (S14)) for an hexagonal-lattice unit cell with dipole-dipole interacting cubes, where the azimuthal orientation of the vertical axis of the central cube is rotated by ω from its equilibrium value, for several values of the center-of-mass distance D between any couple of closest-neighbor cubes. The cube contact angle is 90°, the cube total surface Σ, and the cube side L. The red dotted curves represent the fit around each minimum of $E_7^{*(x)}$ with $a_x(\vartheta^*) + \omega^2\, C_x(\vartheta^*)/2$. ($b$) Values of $C_x(\vartheta^*)$, as obtained for the various D considered. The dotted curve is the fit of these values using $A\, e^{-B/\vartheta^*}$. (c) Contour plots of the interface height profile, as obtained through our numerical method, for the honeycomb-lattice unit cell in the case $D = 1.65\, L$ and for different values of ω. The plane $z = 0$ correspond to the fluid-fluid interface when no cubes are adsorbed.

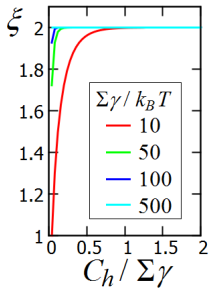

Figure S8: Behavior of $\xi[C_h]$ (Eq. (S8)) for different values of $\Sigma\gamma/k_BT$. As shown, for $\Sigma\gamma/k_BT \geq 100$ we can consider $\xi \approx 2$ always.

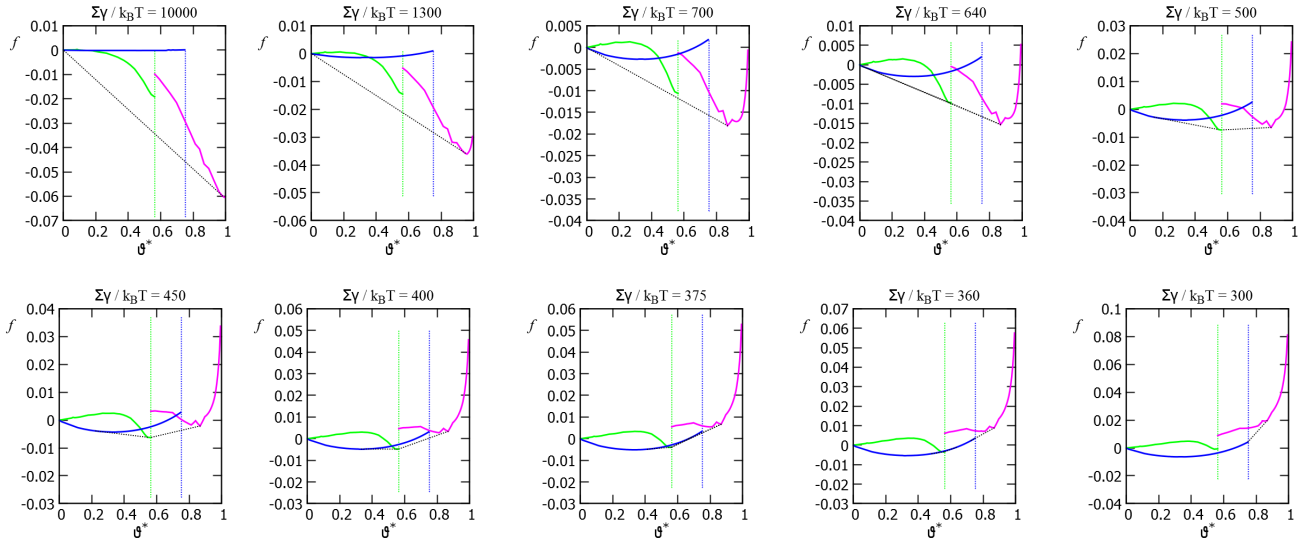

Figure S9: Plots of $F_f(\vartheta^*)/A\gamma$ (Eq. (S5)), $F_h(\vartheta^*)/A\gamma$ (Eq. (S9)), and $F_x(\vartheta^*)/A\gamma$ (Eq. (S12)), in blue, green, and violet lines respectively, with respect to the normalized density ϑ^*, for different values of $\Sigma\gamma/k_BT$. The dotted vertical blue line represents the value of ϑ^* for which the fluid phase can no longer occur. The dotted vertical green line represents the value of ϑ^* corresponding to the closest-packing fraction for the honeycomb-lattice phase. The closest-packing fraction for the hexagonal-lattice phase corresponds to $\vartheta^* = 1$. With black dotted lines we show the presence of common tangents, which indicate phase coexistence.

V. VAN DER WAALS INTERACTIONS

In our work we did not include other possible kinds of particle-particle interactions. So one needs to be aware when they are also relevant, compared to capillarity. Here we address this point for van der Waals forces, showing that, for typical experimental parameters, they are relevant only in the limit of very small particles and very small (almost contact) particle-particle distances. In Fig. S10 we show the van der Waals potential Φ_{vdw} between two spheres of diameter $\sigma \equiv 2R$, with respect to the particle center-of-mass distance $D \equiv d + \sigma$, calculated with a Hamaker-de Boer approach [61] as

$$\Phi_{vdw}(d) = -\frac{A}{6}\left[\frac{2\,R^2}{d^2+4\,R\,d} + \frac{2\,R^2}{d^2+4\,R\,d+4\,R^2} + \ln\left(\frac{d^2+4\,R\,d}{d^2+4\,R\,d+4\,R^2}\right)\right] , \tag{S15}$$

for a system with surface tension $\gamma = 0.02$ N/m and Hamaker constant $A = 0.15$ eV (which is an estimation for a PbSe/Hexane/PbSe system [62]. These values are an order-of-magnitude estimate for the experimental systems in Refs. [26-28], and a more accurate estimation should take into account that the cubes are adsorbed at a fluid-fluid interface and therefore the effective Hamaker constant can be slightly different. We plot $\Phi_{vdw}/2$ in units of $\Gamma\gamma$, where $\Gamma = 4\pi\sigma^2$, such that $\Gamma\gamma \approx 1.5 \cdot 10^5\, k_B T$ for $\sigma = 100$ nm and $\Gamma\gamma \approx 1.5 \cdot 10^3\, k_B T$ for $\sigma = 10$ nm. Compared with the capillary forces in Fig. 2(d), van der Waals interactions are completely negligible for spheres with $\sigma = 100$ nm, while they may become relevant for spheres with $\sigma = 10$ nm, i.e. with size comparable to the nano-cubes in Refs. [26-28]. Note however that the range of capillary interactions goes far beyond the range of van der Waals forces (compare Fig. 2(d) and S10). So, for such experiments, capillarity remains the leading driving force, while van der Waals forces may come into play only when the particles get very close to each other.

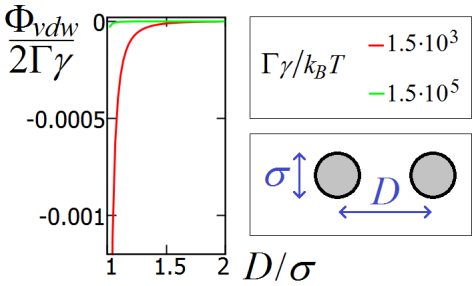

Figure S10: van der Waals interaction potential Φ_{vdw} between two spheres of diameter σ and at a center-of-mass distance D (see Eq. (S15)), for a system with Hamaker constant $A = 0.15$ eV, in units of $\Gamma\gamma$, with $\gamma = 0.02$ N/m and $\Gamma = 4\pi\sigma^2$ the sphere surface area.

VI. CASIMIR-LIKE INTERACTIONS

Another kind of particle-particle interactions that we did not include in our analysis are Casimir-like forces, which arise between adsorbed particles as a consequence of the thermal fluctuations (called capillary waves) experienced by the fluid-fluid interface equilibrium profile. We show here that these forces are indeed negligible compared to the capillary interactions induced by the hexapolar deformations considered in our work.
Following Ref. [63], we can express the fluctuation-induced potential between two spheres adsorbed at a fluid-fluid interface as

$$V_{fluc} \approx -k_B T \frac{R^4}{D^4} \,, \tag{S16}$$

with R the sphere radius and D the distance between the centers of mass of the two spheres. For our cubes (with side L and total surface area Σ) adsorbed at a fluid-fluid interface with surface tension γ, we can use $R \approx L/2$ to rewrite this expression, as an order-of-magnitude estimation, as

$$\frac{V_{fluc}}{\Sigma\gamma} \approx -\frac{k_B T}{\Sigma\gamma} \frac{L^4}{16 D^4} \,. \tag{S17}$$

Using for example $k_B T/\Sigma\gamma \approx 350$, which corresponds to the high-temperature limit for the honeycomb-hexagonal phase-coexistence area in the phase diagram of Fig. 3, and $D = 1.5\,L$, i.e. almost the contact distance for the cubes, we obtain $V_{fluc} \approx 0.000035\,\Sigma\gamma$, which is definitely negligible compared to the cube-cube attractive pair potential $2\tilde{E}_2 = \mathcal{O}(0.01\Sigma\gamma)$ (see Fig. 2(a)).